J Mater Sci (2011) 46:2050–2057
DOI 10.1007/s10853-010-5037-8

Effect of modified MWCNT on the properties of PPO/LCP blend

G. C. Nayak · R. Rajasekar · C. K. Das

Received: 3 August 2010 / Accepted: 26 October 2010 / Published online: 11 November 2010

Abstract In this work we have coated multiwalled carbon nanotubes (MWCNTs) with SiC by solgel process and these modified MWCNTs are dispersed in PPO/LCP blend. The dispersion of these modified MWCNTs are analyzed by FESEM and found to be improved compared to pure MWCNTs. Thermal and mechanical properties of the modified MWCNTs added nanocomposites are higher than that of the pure MWCNTs added nanocomposites. PPO/LCP forms an incompatible blend while addition of unmodified and modified MWCNTs improves the compatibility between the blend partners.

Introduction

The biggest challenge in manufacturing carbon nanotubes (CNTs) based polymer nanocomposites lies in the dispersion of individual CNTs in the polymer matrix, which will expose the maximum interfacial area for interaction with the polymer. To improve the dispersion of CNTs in the polymer matrix both covalent and non-covalent modifications of CNTs were reported in the literature [1–6]. Covalent modification deals with the incorporation of functional groups on the CNTs [7] whereas non-covalent modification involves the wrapping of CNTs with polymers and surfactants [8–10].

However, covalent modification introduces defective sites in the CNTs while the non-covalent approach gives rise to poor bonding between the polymer and nanotubes, which under stress can pulled out of the polymer matrix.

G. C. Nayak (✉) · R. Rajasekar · C. K. Das
Materials Science Centre, Indian Institute of Technology, Kharagpur 721302, India
e-mail: gcnayak_bls@yahoo.co.in

The smooth surface of CNTs and its tendency to form agglomerates limits the effective load transfer from polymer to the fillers. Some papers have been published where different nanoparticles has been deposited on the CNTs, which makes the surface of CNTs rough [11]. This ceramics coating will reduce the van der Walls force of attraction between the CNTs, which is the driving force for the formation of agglomeration. These ceramics coated CNTs can have tremendous application in the field of nanocomposites, which is not yet been explored fully. Yuen et al. [12] studied the effect of TiO_2 coated MWCNTs on the properties of epoxy resin and reported an improvement in the dispersion as well as mechanical properties of the nanocomposites.

In recent years a large amount of research has been focused on the blends of thermoplastics and liquid crystalline polymers (LCP) with and without compatibilizers [13–22]. Baird et al. used functionalized polypropylene, MAH-*g*-PP, as a compatibilizer for the polypropylene/LCP blends and found an improved interfacial adhesion due to some specific interactions like hydrogen bonding [16–18]. Seo demonstrated the compatibilization of PA6/Vectra B950, PA46/Vectra B950, PBT/Vectra A950 blends by MAH-*g*-EPDM. According to Seo, some chemical reaction between MAH groups and LCP were responsible for the compatibilization [14, 19–21]. Recently, nanosilica in PP/LCP blend [22–24], glass beads in PC/LCP blend [25], $CaCO_3$ whiskers in PS/LCP blend [26] were used for the better fibrillation of LCP. In that context CNTs can be used owing to its high aspect ratio and better thermal and mechanical properties.

In this work, we wish to report the effect of SiC coated MWCNTs on the thermo-mechanical properties of PPO/LCP blend matrix. The objective of this work is, SiC coating will produces a very rough surface on the CNTs

which may improve the dispersion of the CNTs in the polymer matrix and also resist the slippage of these tubes from the polymer matrix and improves the mechanical thermal properties.

Basic components

Poly(phenylene oxide) (PPO) was supplied by GE plastic. This has a T_g of about 210 °C. LCP used here is a commercially available nematic and fully aromatic copolyester, Vectra A950, supplied by Ticona (Shelby, NC). Vectra A950 is a copolyester of 73 mol% *p*-hydroxybenzoic acid (HBA) and 27 mol% 2-hydroxy-6-naphthoic acid (HNA). The glass transition and melting temperatures are 110 and 282 °C, respectively.

MWCNTs (MWCNTs-1000) were obtained from IIjini Nano technology, Korea. These MWCNTs are having a diameter of 10–20 nm, length 20 μm and aspect ratio of ~1000. The density of MWCNT is 2.16 g/cm^3. Solid state PCS, for the modification of MWCNTs, are obtained from DMSRDE, Kanpur, having Mw ~1800.

Preparation of SiC coated MWCNTs

SiC coated MWCNTs (S-MWCNTs) are prepared by following the method, already reported in literature [27]. Briefly solid PCS are dispersed ultrasonically in 50 mL of *n*-hexane using a horn type ultrasonicator for 15 min. Then the MWCNTs were added to the PCS containing solution and ultrasonicated at 60 °C for 30 min to disperse the MWCNTs uniformly. The solvent is allowed to evaporate in a draft chamber at 25 °C. Then the MWCNTs and PCS mixture is cured at 240 °C for 90 min and then at 1150 °C for 60 min in a quartz crucible.

Preparation of composites

The formulations of composites are given in Table 1. Prior to mixing PPO and LCP are dried under vacuum at 80 °C and MWCNTs at 300 °C for 12 h. PEI/LCP/MWCNTs composites with pure MWCNTs and S-MWCNTs are prepared by melt blending in a sigma high temperature internal mixture equipped with two Sigma type counter rotating rotors. Blending is carried out at 310 °C and 100 rpm. One set of pure PEI/LCP binary blend also prepared by the same route for comparison. Slabs for the mechanical testing are prepared by compression molding at 320 °C at 10 MPa pressure and allowed to cool to room temperature under the same pressure.

Table 1 Sample codes and formulation of PPO/LCP nanocomposites

Sample code	PPO (wt%)	LCP (wt%)	MWCNTs (wt%)	S-MWCNTs (wt%)
PPL	70	30	–	–
PPLC	69.3	29.7	1	–
PPLS	69.3	29.7	–	1

Characterization

XRD analysis

X-ray diffraction (XRD) was performed with a PW 1840 X-ray diffractometer using copper target (Cu Kα) at a scanning rate of 3 °C/min to check the formation of S-MWCNTs.

Rheology

Rheology study is carried out in a Capillary Rheometer (Smart RHEO 1000, CEAST) at 320 °C, at different shear rates, to investigate the effect of unmodified and modified MWCNTs on the viscosity of PEI/LCP blend.

Mechanical properties

Tensile tests are carried out on dumb-bell shaped samples using a Hounsfield HS 10 KS (universal testing machine) operated at room temperature with a gauge length of 35 mm and crosshead speed of 5 mm/min. Tensile values reported here are an average of the results for tests run on at least four specimens.

Fracture surface analysis

Fracture surfaces are analyzed by Scanning Electron Microscope (Tescan, Vega LSU) to reveal the fracture mechanism of the blend systems. Before the analysis samples are gold coated to make it conducting.

Field emission scanning electron microscopy (FESEM)

A Carl Zeiss-SUPRA^{TM} 40 FESEM with an accelerating voltage of 5 kV is employed to observe the morphology of the tensile fractured nanocomposites. A thin layer of gold was sputtered on the fractured surface of the specimens for electrical conductivity.

Dynamic mechanical thermal analysis (DMTA)

Dynamic mechanical analyses of binary and ternary blends are done by a TA Instrument (DMA 2980 model) in single cantilever bending mode. The storage modulus (E'), loss

modulus (E'') and tan δ are recorded at a frequency of 1 Hz from ambient to 250 °C and at a heating rate of 5 °C/min.

Thermogravimetric analysis

Thermogravimetric analysis (TGA) curves were recorded with a Dupont 2100 Thermogravimetric analyzer. The TGA measurements were conducted with a heating rate of 10 °C/min under air atmosphere from 50 to 650 °C.

Results and discussion

XRD study of S-MWCNTs

XRD pattern of PCS, MWCNTs, and S-MWCNTs were depicted in Fig. 1a. Pure PCS showed a broad peak around $2\theta = 10°$, whereas no such peak was observed after the modification of MWCNTs with PCS (S-MWCNTs). However, appearance of new peaks at certain angles (as shown in Fig. 1a) confirms the formation of β-SiC. This suggests that PCS had been decomposed completely to form β-SiC particles. In comparison with MWCNTs the peak intensities of S-MWCNTs (especially at $2\theta = 27°$) had been increased, which may be due to the removal of impurities like amorphous carbon during pyrolysis carried out at 1150 °C.

Figure 1b shows the XRD plots of blend systems along with pure PPO and LCP. As can be seen pure PPO shows a broad peak which corresponds to its amorphous nature while pure LCP shows a sharp peak, indicating its crystalline nature. Binary blend, PPL, is showing peaks for both PPO and LCP and have a crystallinity of 17%. Incorporation of MWCNTs increases the crystallinity of the nanocomposite (PPLC) to 22% while addition of S-MWCNTs shows 26% crystallinity. This increase in crystallinity is due to the nucleating ability of the nanofillers.

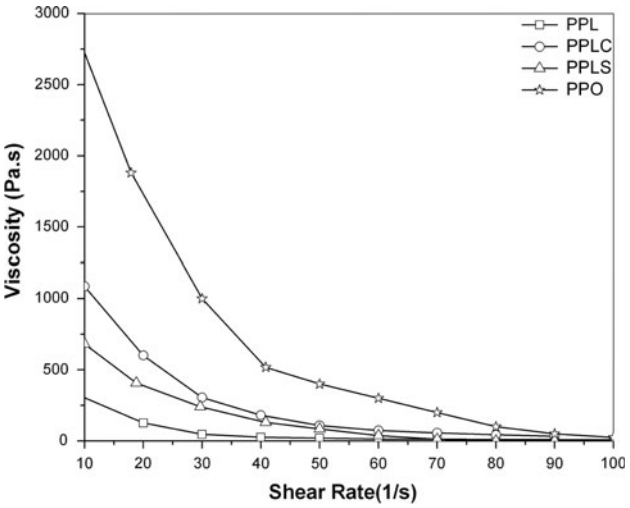

Fig. 2 Viscosity versus shear rate plot of blend systems

Rheological study

The rheological properties of the nanocomposites are shown in Fig. 2. The viscosity of pure PPO along with binary and ternary blends decreased with increasing shear rate, i.e., all the systems shows shear thinning effect. This effect is due to the reduced entanglement density of polymer chains under the shear stress which leads to the lowering of viscosity [16]. Blending of LCP with PPO, significantly reduces the viscosity of PPO which may be due to the interlayer slippage between the LCP and PPO phase. Incorporation of MWCNTs and S-MWCNTs in PPO/LCP blends enhances its viscosity; however, in comparison with pure PPO their viscosities are found to be quite lesser, which implies the improvement in processability of the nanocomposites. Among the nanocomposites, the MWCNTs filled system has higher viscosity compared to S-MWCNTs filled system. The lower viscosity of the S-MWCNTs filled system may be due to the enhanced fibrillation of LCP. Under higher shear rate, these LCP

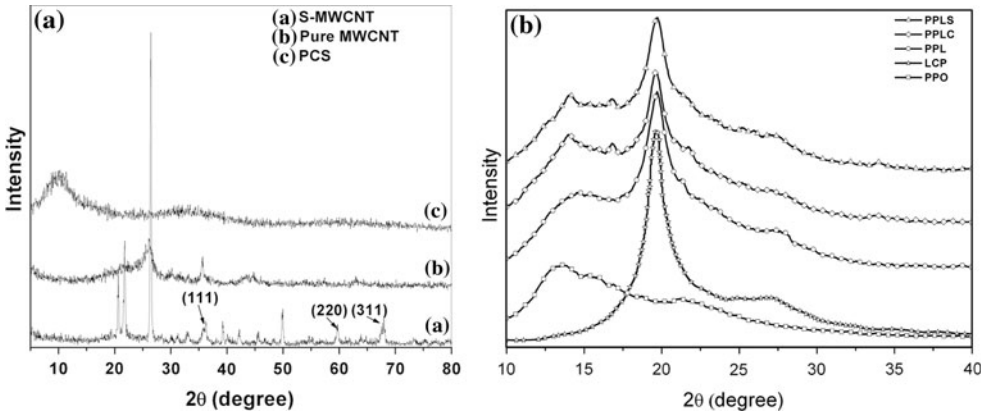

Fig. 1 **a** XRD pattern of PCS, pure MWCNTs, and S-MWCNTs. **b** XRD pattern of blend systems

fibers are being aligned in the direction of flow results in lower viscosity of S-MWCNTs filled system compared to MWCNTs filled system.

Mechanical properties

The results obtained from the tensile experiment of PPO/LCP blend with and without MWCNTs are depicted in Table 2. For each set five samples are tested and the results presented are the average of these values. As evident from Table 2, blending LCP with PPO lower the tensile strength of binary blend compared to pure PPO. This may be due to the incompatibility between the blend partners. Incorporation of MWCNTs increases both tensile strength and modulus of the nanocomposite compared to the binary blend system. There is an improvement of 52 and 27% in tensile strength and modulus, respectively, of PPLC compared to PPL, with an addition of only 1 wt% of MWCNTs. This enhancement of tensile properties can be ascribed to reinforcing ability of MWCNTs. The improvement of tensile properties becomes more pronounced in PPLS (88 and 40% for tensile strength and modulus) due to the better distribution of S-MWCNTs, at the PPO/LCP interface (discussed in FESEM section), compared to pure MWCNTs in the blend matrix. This better distribution of S-MWCNTs at the interface decreases the pullout of LCP domains from the PPO phase and also improves the load transfer from the PPO to the rigid LCP phase as a result both tensile strength and modulus increases.

SEM analysis

To reveal the possible mechanism of reinforcement, the failure surfaces of nanocomposites are analyzed by SEM. The SEM images are presented in Fig. 3a–c and the magnified section of the images are shown in Fig. 3d–f. Binary blend of PPO/LCP shows globular structure of LCP dispersed in the PPO matrix. A large gap around the LCP globules shows that PPO and LCP formed an incompatible blend. Due to the incompatibility between PPO and LCP, the spherical domains of LCP are pulled out of the PPO phase during tensile test (evident from the holes created after pullout of LCP phase) which decreases the tensile strength of PPL compared to pure PPO. Incorporation of MWCNTs decreased the domain size of dispersed LCP globules and reduced the pullout of LCP phase due to the presence of MWCNTs at the interface of PPO and LCP which act as a bridging agent between the two phases. The average domain size of LCP is lowest in PPLS which results in improved tensile strength. Another interesting observation is the surface of the LCP domains are smooth incase of PPL system which indicating towards the incompatibility between the blend partners (Fig. 3d). However, in PPLC and PPLS the LCP surfaces are not smooth and shows some fibrous structure which pointing towards the increase in compatibility between the blend partners in presence of MWCNTs and S-MWCNTs (Fig. 3e, f). A few broken LCP domains are also observed in case of PPLC and PPLS which exposed the flower like morphology. This broken LCP domain suggests that load has been transferred to the rigid LCP domains in presence of MWCNTs and S-MWCNTs. Due to this phenomenon the mechanical properties is higher for the nanofillers added systems.

Table 2 Tensile properties of PPO/LCP nanocomposites

Sample code	Tensile strength (MPa)	Elongation at break (%)	Young's modulus (MPa)
PPO	45 ± 4	4.3 ± 0.3	1323 ± 13
PPL	36 ± 3	3.21 ± 0.9	1376 ± 22
PPLC	55 ± 5	2.43 ± 1.6	1752 ± 31
PPLS	68 ± 3	2.14 ± 1.4	1934 ± 28

FESEM

Figure 4a and b shows the FESEM image of MWCNTs and S-MWCNTs. As can be seen pure MWCNTs is having a very smooth surface with a diameter of about 40 nm while S-MWCNTs is having a rough surface with a diameter of about 80 nm. This increase in diameter of MWCNTs is due to the SiC coating. This result is in accordance with the XRD results where peaks for the β-SiC was observed.

Since MWCNTs has a smooth surface, during melt blending polymer chains may slip past the nanotubes surface which makes it difficult to get an uniform dispersion. However, S-MWCNTs is having a very rough surface (due to the SiC coating) which will anchored the polymer chains and reduces the slippage of polymer chain. This factor is important for the improvement of dispersion of S-MWCNTs in the matrix because when they are melt blended the matrix will drag the S-MWCNTs along the flow direction (due to the physical anchoring of polymer chains at the interface) and helps in achieving a better distribution. To confirm the state of dispersion of MWCNTs in the blend matrix FESEM analysis of fractured surfaces are done at higher magnification. Figure 4c and d shows the FESEM images of PPLC and PPLS. As can be seen from Fig. 4c agglomeration of MWCNTs is formed in PPLC while dispersion of S-MWCNTs has improved in PPLS (Fig. 4d) compared to pure MWCNTs. Amount of S-MWCNTs at the PPO/LCP interface is more compared to pure MWCNTs which resist the dragging out of LCP phase from the PPO phase by bridging the two phases and hence increase its mechanical properties.

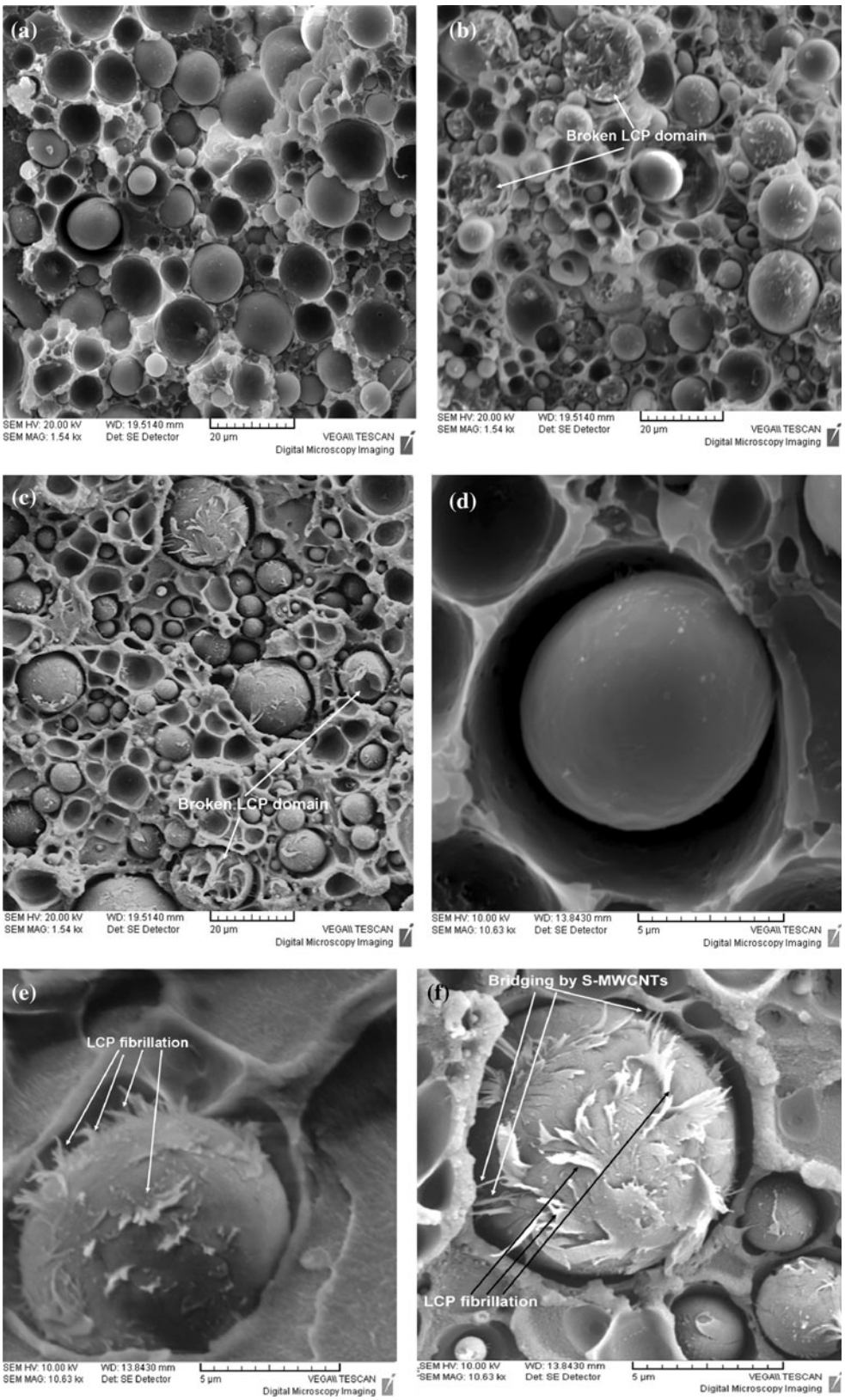

Fig. 3 **a** Fracture surface of PPL (low magnification). **b** Fracture surface of PPLC (low magnification). **c** Fracture surface of PPLS (low magnification). **d** Fracture surface of PPL (higher magnification). **e** Fracture surface of PPLC (higher magnification). **f** Fracture surface of PPLS (higher magnification)

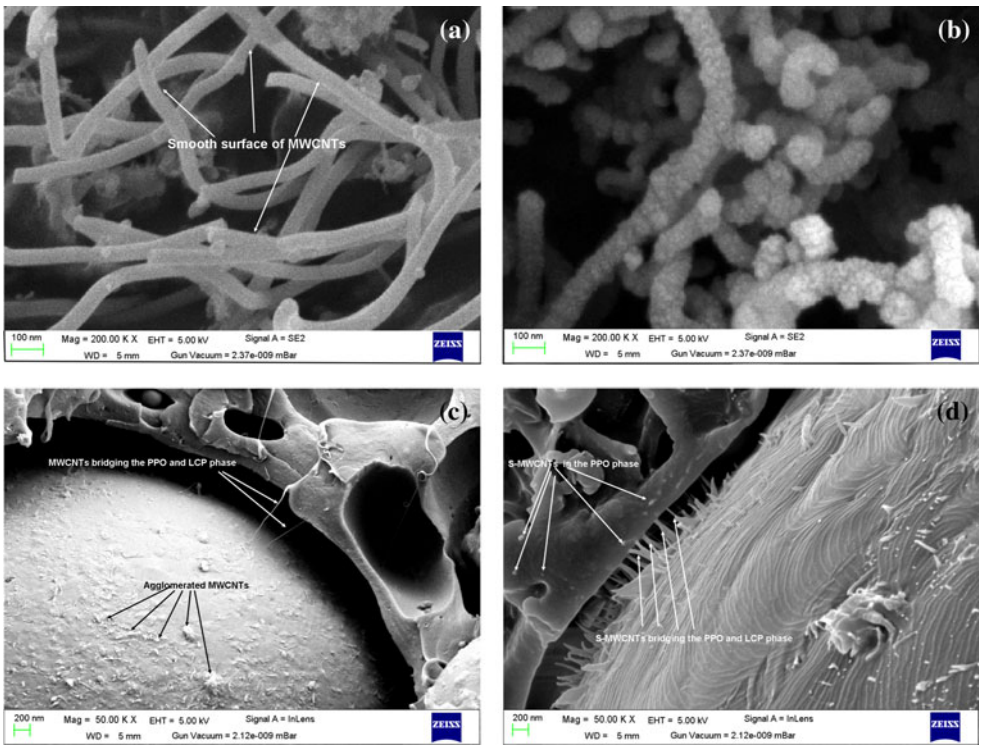

Fig. 4 **a** FESEM image of unmodified MWCNTs. **b** FESEM image of modified MWCNTs. **c** FESEM image of PPLC. **d** FESEM image of PPLS

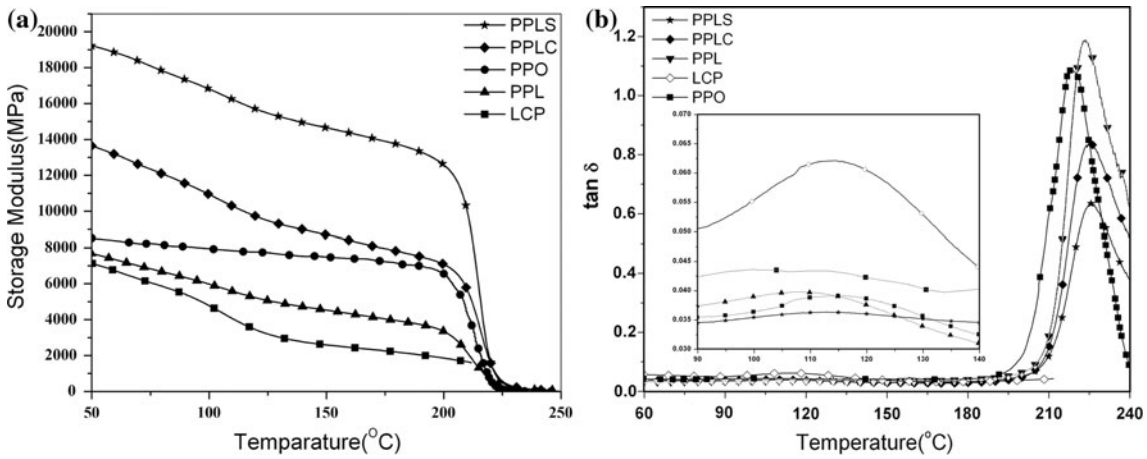

Fig. 5 **a** Storage modulus plot of blend systems. **b** Tan delta plot of blend systems

DMTA study

Figure 5a shows the storage modulus of binary and ternary blends along with pure PPO as a function of temperature. From the figure it is clear that storage modulus of PPO/LCP binary blend is lower as compared to pure PPO. This can be attributed to the incompatibility of PPO/LCP phases. Same observation was reported by Sahoo et al. [28] where addition of LCP to the PBT matrix shows a downward trend up to 40% LCP contain. Incorporation of MWCNTs increases the storage modulus of the ternary blend PPLC above both PPL and pure PPO. This improvement can be ascribed to the stiffening effect imparted on the polymer blend matrix by the MWCNTs. However, maximum enhancement of storage modulus is achieved by the addition of S-MWCNTs. This increase in modulus can be due to the finer dispersion of S-MWCNTs in the blend matrix (as discussed in FESEM section) due to which the effective interaction area between polymer and nanotubes increased significantly whereas, incorporation of MWCNT forms agglomerates in the blend system, hence the interaction area between the filler and the polymer was

quite lesser, that do not have more pronounced effect on the modulus compared to the system containing S-MWCNTs. Another factor which might have role in the increase in the modulus is the particle size of LCP. From the SEM images it is clear that the particle size of LCP and the gap around LCP domains decreases in the order PPL, PPLC, and PPLS. This reduced particle size and gap around LCP droplets can increase the load transfer from the PPO to the LCP phase which contributes towards the enhancement of storage modulus.

Figure 5b shows the tan δ versus temperature plots for the binary and ternary blends. There is a very minor change in the T_g of PPL compared to pure PPO. But incorporation of MWCNTs and S-MWCNTs shifts the T_g of PPLC and PPLS to higher temperature. The tan δ peak height of PPLC is lower than the binary blend of PPO/LCP which indicates that the heat buildup is lesser in PPLC as compared to PPL which favors the improved damping properties. But PPLS shows the lowest tan δ peak height among all the blend systems which suggests that the incorporation of S-MWCNTs increase the damping behavior of the nanocomposite and also allows better stress transfer from filler to matrix permitting only a small part of it to strain the interface.

TGA

Thermal stability of the PPO/LCP/MWCNTs nanocomposites was determined by TGA and the thermograms are given in Fig. 6. Binary blend of PPO/LCP (PPL) shows two-step degradation. The first step corresponds to the decomposition of PPO component while the second step corresponds to the LCP component. According to Li, thermal degradation of PPO starts at around 430° with the cleavage of ether bond and simultaneous removal of methyl group in the form of methane with the hydrogen being supplied by other methyl groups and benzene ring [29]. Sate et al. [30] demonstrated that, the rapid degradation of LCP starts at 550° with the elimination of H_2O and CO_2. The results of TG analysis are presented in Table 3. The initiation temperature of thermal degradation based on an extrapolation method was found to be 440 and 556 °C (first and second degradation, respectively) for the binary blend (PPL). Incorporation of MWCNTs increases decomposition temperature of first and second steps to 459 and 574 °C, respectively. However, addition of S-MWCNTs shows an improvement to 472 and 585 °C. This enhancement in the thermal stability of the nanocomposites can ascribed to the following factors:

(1) Restriction imposed by the nanotubes on the polymer chains mobility which will reduce the tension induced by the thermal excitation of the C–C bond and leads to an enhancement of the thermal stability [31].
(2) Char formed during the degradation acts as a physical barrier between the polymer and the superficial zone where the combustion of the polymer is occurring thus hinder diffusion of the degradation products from the bulk of the polymer into the gas phase [32].
(3) Finer dispersion of nanotubes in the polymer matrix will increase the interfacial interaction between the CNTs and polymer which will increase the activation energy of decomposition and leads to enhanced thermal stability of nanocomposites [33].

The temperatures for the 5, 10, and 50% weight loss of binary and ternary blends are presented in Table 3. These data indicates a clear improvement of thermal stability of nanocomposites as compared to the binary blend of PPL. Higher thermal stability of the PPLS, compared to PPLC, is due to the improved dispersion of S-MWCNTs (as discussed in FESEM section). Figure 6 shows that the char content of S-MWCNTs added nanocomposites is higher than that of the MWCNTs added system which also contributing towards the improved thermal stability of the PPLS compared to pure MWCNTs in the blend matrix.

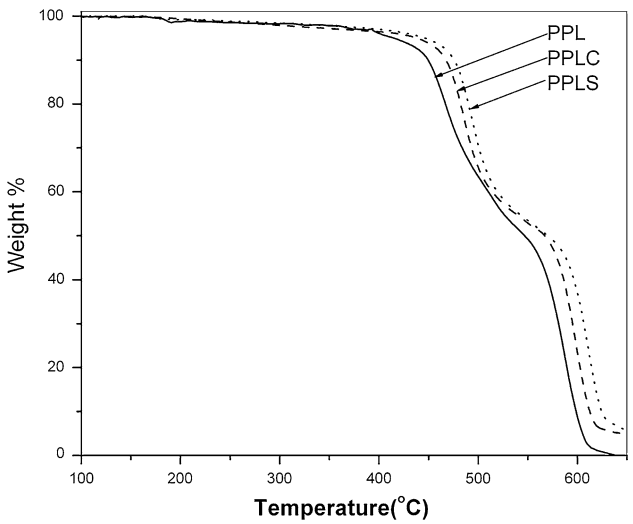

Fig. 6 Thermal stability of blend systems

Conclusion

SiC coated MWCNTs are prepared successfully by solgel process from the solid PCS. XRD confirms the formation of β-SiC particle. Pure and SiC modified MWCNTs are dispersed in the PPO/LCP blend by melt mixing. SiC coating improves the dispersion of modified MWCNTs compared to pure MWCNTs. This improved dispersion results in enhanced thermal stability of the S-MWCNTs added nanocomposites compared to pure MWCNTs added system. Incorporation of pure MWCNTs increase

Table 3 Thermal properties of PPO/LCP nanocomposites

Sample code	Temperature at (°C)				
	First degradation	Second degradation	5% wt loss	10% wt loss	50% wt loss
PPL	440	556	413	449	546
PPLC	459	574	437	467	566
PPLS	472	585	446	476	570

the mechanical properties of ternary blend compared to binary blend of PPO/LCP. But the enhancement in the mechanical properties is more pronounced with the S-MWCNTs added nanocomposites. FESEM analysis confirms the improved dispersion of S-MWCNTs in the blend matrix. Presence of MWCNTs and S-MWCNTs at the interface of PPO and LCP reduces the LCP pullout during mechanical testing which in turn improves the mechanical properties.

References

1. Sumanasekera GU, Allen JL, Fang SL, Loper AL, Rao AM, Eklund PC (1999) J Phys Chem B 103:4292
2. Liu J, Rinzler AG, Dai H, Hafner JH, Bradley RK, Boul PJ, Lu A, Iverson T, Shelimov K, Huffman CB, Macias FR, Shon YS, Lee TR, Colbert DT, Smalley RE (1998) Science 280:1253
3. Mawhinney DB, Naumenko V, Kuznetsova A, Yates JT, Liu J, Smalley RE (2000) J Am Chem Soc 122:2383
4. Dujardin E, Ebbesen TW, Krishnan A, Treacy MMJ (1998) Adv Mater 10:611
5. Vaccarini L, Goze C, Aznar R, Micholet V, Journet C, Bernier P (1999) Synth Met 103:2492
6. Nagasawa S, Yudasaka M, Hirahara K, Ichihashi T, Iijima S (2000) Chem Phys Lett 328:374
7. Hirsch A, Vostrowsky O (2005) Top Curr Chem 245:193
8. Coleman JN, Khan U, Blau WJ, Gun'ko YK (2006) Carbon 44:1624
9. Breuer O, Sundararaj U (2004) Polym Compos 25:630
10. Gacitua W, Ballerini E,A, Zhang A,J (2005) Maderas Ciencia y tecnología 7:159
11. Vairavapandian D, Vichchulada P, Lay MD (2008) Anal Chim Acta 626:119
12. Yuen SM, Ma CM, Chuang CY, Hsiao YH, Chiang CL, Yu Ad (2008) Compos Part A 39:119
13. Seo Y, Hong SM, Hwang SS, Park TS, Kim KU, Lee S, Lee J (1995) Polymer 36:515
14. Seo Y, Hong SM, Kim KU (1997) Macromolecules 30:2978
15. Dutta D, Weiss RA (1992) Polym Compos 13:394
16. Datta A, Chen HH, Baird DG (1993) Polymer 34:759
17. Datta A, Baird DG (1995) Polymer 36:505
18. O'Donnell HJ, Baird DG (1995) Polymer 36:3113
19. Seo Y (1997) J Appl Polym Sci 64:359
20. Seo Y, Kim KU (1998) Polym Eng Sci 38:583
21. Seo Y (1998) J Appl Polym Sci 70:1589
22. Zhang L, Tam KC, Gan LH, Yue CY, Lam YC, Hu X (2003) J Appl Polym Sci 87:1484
23. Lee MW, Hu X, Li L, Yue CY, Tam KC (2003) Polym Int 52:276
24. Lee MW, Hu X, Li L, Yue CY, Tam KC, Cheong LY (2003) Comput Sci Technol 63:1921
25. Chen P, Chen J, Zhang B, Zhang J, He J (2006) J Polym Sci B 44:1020
26. Chen J, Chen P, Wu L, Zhang J, He J (2006) Polymer 47:5402
27. Bose S, Mukherjee M, Pal K, Nayak GC, Das CK (2009) Polym Adv Technol 21:272
28. Sahoo NG, Das CK, Pandey KN, Mathur GN (2002) Mater Lett 56:194
29. Li XG (1999) J Appl Polym Sci 71:1887
30. Sate H, Kikuchi T, Koide N, Furuya K (1996) J Anal Appl Pyrolysis 37:173
31. Chatterjee A, Deopura BL (2006) J App Polym Sci 100:3574
32. Kashiwagi T, Grulke E, Hilding J, Harris R, Awad W, Douglas J (2002) Macromol Rapid Commun 23:761
33. Marosfői BB, Szabó A, Marosi Gy, Tabuani D, Camino G, Pagliari S (2006) J Therm Anal Calorim 86:669